12-1-2017

A Miniature Acoustic Device for Tracking Small Marine Animals or Submerged Drifters

Godi Fischer
University of Rhode Island, fischer@uri.edu

Thomas Rossby
University of Rhode Island, trossby@uri.edu

Daniel Moonan
University of Rhode Island

Citation/Publisher Attribution

Fischer, G., Rossby, T., & Moonan, D. (2017). A miniature acoustic device for tracking small marine animals or submerged drifters. Journal of Atmospheric and Oceanic Technology, 34(12), 2601-2612. 10.1175/JTECH-D-17-0127.1
Available at: http://dx.doi.org/10.1175/JTECH-D-17-0127.1

A Miniature Acoustic Device for Tracking Small Marine Animals or Submerged Drifters

A Miniature Acoustic Device for tracking small Marine Animals or submerged Drifters

G. Fischer*, *Dept. of Electrical Engineering. University of Rhode Island, Kingston, RI 02881*

T. Rossby, *Graduate School of Oceanography, University of Rhode Island, Kingston RI 02881*

D. Moonan, *Dept. of Electrical Engineering. University of Rhode Island, Kingston, RI 02881*

_____

* Corresponding author

ABSTRACT

This paper presents an acoustic archival tag capable of tracking small marine animals. It is also a technology that can be ported to other platforms such as next generation acoustic and Argo floats as well as gliders. Tracking is achieved by standard RAFOS triangulation using the arrival times of unique sound signals emitted by moored sources. At the core of the tag is a custom microchip, which controls all system operations. It incorporates the critical acoustic arrival time detector, a thermal sensor and a pressure sensor interface. All electronic components are housed inside a cylindrical hydrophone of 25.4 mm length and 10.7 mm diameter. The collected data is archived in nonvolatile memory chips with a total capacity of 4 Mb, sufficient storage to record position, temperature and pressure on an hourly basis for two years. The tag consumes 4-5 μW in standby mode and between 60-90 μW while the sound arrival time detector is in operation. The power is provided by two button cell silver-oxide batteries, which enable an active tag lifetime of approximately two years.

1. Introduction

Fish biologists have an urgent need to better understand the life cycle and dynamics of various life forms in the sea and how these depend upon their environment and interact with each other. This is of particular concern to commercially important species such as the wide-ranging tuna at/near the surface, benthic species such as cod, halibut and flounder and lobster that live at the bottom. What are the temporal and spatial scales associated with their life cycles? Where and when are these populations most vulnerable; what might be done to enhance their recruitment, enhance survival, and maximize sustainable fishery production? These are not new questions, of course, and indeed much information has been obtained about their behavioral patterns by means of various kinds of data storage tags (DST) that are attached either externally to the dorsal side of the animal, or subcutaneously.

For an individual fitted with a DST, by logging in-situ physical parameters, e.g., temperature, depth and light intensity, geographical position is inferred on the basis of retrospective analysis of known hydrographic features of the animal's environment or light level for surface species. Such retrospective positioning is necessarily imprecise because physical features may vary only slightly (horizontally, and vertically in higher latitudes) or be poorly known (at least for purposes of retrospective positioning). These limitations notwithstanding, much has been learned with existing DST designs.

For example, the use of DSTs has been pioneered for nearly a decade in studies of bluefin tuna (e.g. Gunn and Hartog, 1999, Block et al. 2001), providing crucial insight on behavior, physiology, and movements. Metcalfe et al. (1994) demonstrated and described selective tidal stream transport in European plaice, a flatfish, in the North Sea. While DSTs have provided a lot of original insights, accurate positioning remains elusive for the reasons stated. This limitation has to a significant degree been relaxed thanks to a new technology whereby tiny high frequency acoustic transmitters, each transmitting a unique ID code, are attached to fish. These devices are not DSTs in the usual sense, but when a fish tagged with such a transmitter passes within acoustic range of a moored stationary receiver, a record of that event is kept. While fish cannot be tracked continuously, this widely used technology gives valuable insight into the overall range and timing of their movements (VEMCO, 2009, Gazit et al., 2013).

In this paper we describe the development of state-of-the-art technology to track fish continuously over a wide range of distances. Two technologies make this development possible. The first is an acoustic navigation concept in the ocean known as RAFOS (Ranging And Fixing Of Sound), and the second is cost-effective access to customer-design microchip technology. The first, RAFOS, is widely used to determine the trajectories of free drifting subsurface floats (aka RAFOS floats), the movements of which can be determined from the arrival times of specially programmed acoustic signals transmitted from distant sound sources. Unlike the older SOFAR float system (see section 2), the reversed role of transmitter and receiver in the RAFOS float system makes it possible to deploy just a few stationary sound sources as navigation beacons, whose very low frequency transmissions, centered at 260 Hz, can be heard at $10^2 – 10^3$ km distances depending on acoustic propagation conditions and source power (Rossby et al., 1993). The peak sound pressure level generated by a RAFOS source is close to 180 dB re μPa @ 1 m. This value is on par with the pressure level generated by some whales and is not expected to harm marine life (Parvin et al., 2007). The second technology, customer-design microchip technology, allows for the development of electronic-chips designed to provide specific functionality, in our case an acoustic receiver and data logger that can operate at extremely low power for several years.

2. Background

A truly remarkable property of the ocean is its acoustic transparency (Urick, 1984). This property has been used for many purposes such as echo sounding, fish localization, antisubmarine warfare, acoustic thermometry of the oceans, and the tracking of sub-surface drifters over great distances.

The existence of the deep sound channel or SOFAR (sound fixing and ranging) channel has allowed for the localization of sound sources at distances well in excess of 1,000 km. Oceanographers have used floats extensively to trace the movement of water parcels as they are carried by ocean currents (e.g. Bower et al., 1995, Rossby, 1996). In the early years, the floats were acoustic transmitters (aka SOFAR floats, Rossby et al., 1975) with signals that could be picked up at shore-based hydrophones and later on autonomous moorings. With the advent of low-power microprocessors in the late 1970s, it became possible to shrink the entire acoustic receiver and signal processing onto a small circuit board leading to a much-reduced cost of the floats. The data collected in the RAFOS floats are transmitted back via satellite for analysis at the end of the float's underwater mission (Rossby et al., 1986).

The actual process of detecting the arrival time of an acoustic signal is quite straightforward and is an almost entirely digital process. The traditional SOFAR/RAFOS float signal consists of a linear increase in frequency from 259.38 Hz to 260.90 Hz over 80 seconds. After the incoming signal is amplified, band-shifted to zero frequency and clipped, it consists of a single-bit stream reflecting whether it is positive or negative, essentially a one-bit phase digitization. The receiver knows the expected binary sequence, so the remaining step is to compare the incoming, 80-second-long bit stream to the expected pattern. This process is known as a cross correlation or exclusive NOR (XNOR) operation in digital terms. The time at which the best fit occurs is considered to be the time of arrival of that signal. Since all emitted signals are identical regardless of sound source location, their identity is established based on arrival times recorded in previous listening windows combined with the projected float movement. This source identification is carried out retrospectively, the receiver simply stores the arrival times.

The RAFOS technology has been immensely successful; well over 1,000 floats have been deployed over the 30+ years they have been in use. Here we take this technology a step forward by shrinking the entire functionality of the RAFOS float onto a single monolithic chip, which becomes the nerve center of the fish-tag. The next section describes the architecture, design considerations and functionality of the newly developed fish-tag.

3. The Fish Tag

3a. Tag architecture

Figure 1 depicts the basic functional components of the tag. At the core of the system is an application specific integrated circuit (ASIC), which performs all control functions, including instructing the tag to execute a specific sampling protocol, calibrating the temperature sensor and the timing unit as well as storing the recorded data in external non-volatile memory chips. The current system can address up to 4 memory chips with a capacity of 1 Mb each. Upon completion of the calibration and programming phase, the 3-wire interface to the host PC is removed so that the tag can be sealed and made ready for deployment. The tag also houses a commercial micro-machined pressure sensor to record depth. The 2 mm x 2 mm sensor provides a range of 300 PSI (~200 m depth). Due to the potentially large raw sensor offset of as much as 1/3 of its full range,

the pressure sensor interface aboard the ASIC has been configured to accommodate more than twice the nominal sensor range. This reduces the resolution from potentially 0.3 PSI to 0.75 PSI (~0.5 m depth), but eliminates a pre-calibration procedure. The actual sensor offset and gain values are recorded only after the tag's retrieval. Actually, offset is known since the tag is in operation before the fish is released, so it is primarily the gain factor that needs to be determined. Knowing sensor gain and offset enables a precise digital calibration of the archived pressure values. The resulting accuracy depends, of course, on how well offset and gain at the actual sampling time match their post-retrieval values.

The monolithic thermal sensor makes use of the temperature characteristic of a PN-junction (Vittoz and Neyroud, 1979). This solution provides for a small silicon foot print, but, similar to the pressure sensor, it suffers from relatively poor device-to-device matching. To mitigate the potentially large temperature offset errors, the sensor has been complemented by a 7-bit digital calibration unit, which keeps the maximum raw error below 0.3°C. Keeping this raw error small is important, because the pre-calibrated thermal output is used to compensate for the temperature induced frequency deviations of the master timing crystal as discussed in section 3d. A post retrieval temperature calibration will reduce the absolute error close to ± 0.05°C.

The remaining two functional components of the tag are the hydrophone and the electric power source. The cylindrical hydrophone, being the largest component, also serves as the housing for all electronic components. The copolymer hydrophone utilized by the prototype tags is a cylinder of 25.4 mm length and 10.7 mm outer diameter. Its hydrostatic sensitivity is listed as -195 dB re 1V/μPa.

The tag is powered by two series connected silver-oxide button cells with a nominal terminal voltage of 1.5 V and a capacity of 80 mAh. With a diameter of only 7.9 mm, the batteries fit tightly inside the hydrophone cylinder. The center tap of the 2 batteries serves as the common voltage to enable a bipolar voltage swing of ±1.5 V.

The most critical unit of the tag is arguably the sound arrival time detector, in particular the analog receiver section. The next subsection describes this unit in more detail.

3b. Acoustic Receiver

By necessity, long-range acoustic tracking requires working at very low frequency somewhere between 200 Hz and 800 Hz (e.g. Urick, 1983). RAFOS and the earlier SOFAR floats have very successfully operated at 260 Hz in a wide variety of environments (Rossby, 2007). Regardless of specific design, most low frequency sound sources utilize a long pipe to achieve efficient acoustic radiation over a very narrow range of frequencies, typically less than 3 Hz.

The acoustic signature of the fish tag has been chosen different from the traditional RAFOS system to better cope with a more dynamic target like a fish versus a float. The frequency modulation range or signal bandwidth has been increased from 1.52 Hz to 3 Hz and the duration of the signal has been reduced from 80 to 32 seconds. This renders the tag less vulnerable to Doppler induced frequency shifts and reduces arrival time or distance errors cause by the relative

target motion by a factor of 5. In addition, the signal center frequency has been slightly increased from 260 to 262 Hz so that a 256 Hz frequency modulation can shift the signal center to 6 Hz (Fischer et al, 2006). This allows the final 1-bit digitizer to be clocked at a much lower rate of 32 Hz. This low clock frequency not only saves power but also significantly reduces the size of the digital memory required by the subsequent arrival time detector. The proximity of the fish tag frequency range to the RAFOS transmission makes it possible to use existing RAFOS sources retuned to match the 0.7% higher transmission frequency.

By implementing the narrow band filter cascade of the fish tag receiver with analog sampled-data circuits (Schneider and Galup-Montoro, 2010; Crols and Steyaert, 1994), all filter characteristics scale as the sampling rate. This opens the possibility of reducing the minimum time step of the arrival time detector by simply clocking all sampled data filter sections at a higher rate. This does, of course, require the acoustic signal to be centered at a correspondingly higher frequency. Altering the filter clocks can readily be achieved by complementing the crystal oscillator with a low power phase-locked loop designed to generate a range of integer fractions (e.g. n/4, n={5,6,7,8}) of the original crystal frequency (Fischer and Luo, 2012).

Figure 2 shows a measured spectral response of the acoustic receiver. The plot has been generated via of a 1-million point FFT using a sampling rate of 10 kHz. To obtain this 100-second long recording, a 262 Hz sinusoid of 500 nV amplitude was directly fed into the first stage of the filter cascade. The data was collected by a digital oscilloscope. The amplified signal component is clearly visible in the spectral plot. The power of the displayed in-band noise, that is the sum of all spectral components between 4.5 Hz and 7.5 Hz with the exception of the 262 Hz signal, amounts to -42.8 dB. This corresponds to an equivalent noise voltage of 7.2 mV. Dividing this voltage by the nominal receiver gain of 18,000 (85 dB) yields an equivalent input referred noise voltage of 400 nV. The ambient noise voltage picked up by the copolymer hydrophone with a sensitivity of -195 dB re 1V/μPa is expected to be somewhere between 400 nV and 4 μV depending on sea state and other environmental conditions (Wenz, 1962; Urick, 1984; Harrison, 1996). The receiver self-noise is therefore not expected to limit the detection range.

3.c Arrival Time Detector

To find a reliable estimate for the arrival time of a specific sound signature, in this case a narrow band linear frequency sweep, the detector compares the digital output stream of the acoustic receiver to a stored replica of the expected signature. The time corresponding to a maximum overlap between the two signals constitutes the best estimate for the arrival time. By quantizing the signal at the end of the receiver cascade to one bit, this comparison can be carried out by a single logic XNOR gate as stated in section 2. The output bit stream of this gate is then fed into a binary counter, which accumulates the number of matched pairs over a length of 1024 samples. To accomplish this in real time, the counter needs to be clocked 1024 times per output period. The nominal output rate of 32 Hz thus requires a correlator clock rate of 32.768 kHz. This value is particularly convenient, since it is the clock frequency used by almost all electronic watches. Watch crystals are widely available and inexpensive.

Figure 3 illustrates the efficacy of the described cross-correlation procedure. Since the micro-chip does not allow a direct observation of the correlator function, we resorted to a simulation to illustrate the applied procedure. The top left window in **Figure 3** shows an ideal receiver output over a full signature length of 32 seconds or 1024 samples. The window below represents a more challenging scenario with two acoustic signatures arriving just 0.4 seconds apart (a 98.8% overlap in time) and deeply embedded in noise. In fact, the depicted in-band noise power exceeds each signal power by a factor of 4. This corresponds to a signal-to-noise ratio (SNR) of -6 dB. The top right window depicts the output of the digital cross correlator. To avoid filling the 4 available memory slots per acoustic listening window with correlation peaks pertaining to the same event and so preventing the detection of weaker signatures, a peak detector has been added, which only records the maximum of 16 consecutive correlation values. This 16-sample or 0.5-second-long window is triggered by any correlation value larger than 0.1875. Lower values are disregarded since they are not very different from random correlation spikes caused by the stochastic receiver output noise. The stated threshold corresponds to 608 matches out of 1024 (59.4%). Since the peak detection operates in parallel with the correlation counter, it does not skip any correlation values and thus provides a continuous record of all relevant peaks in the correlator function. The bottom right window in **Figure 3** reveals that the simulated peak detector identified two distinct maxima separated by 0.4375 seconds. This is one sampling period more than the actual signature separation of 0.4 seconds. The fact that each maximum in the bottom right plot is flanked by a number of prominent side peaks underlines the need for a peak detector.

Correctly identifying and timing the relevant correlation peaks does not necessarily lead to a correct geographic position. Doppler frequency shifts caused by the relative velocity between source and receiver can move a fraction of the signal spectrum out of band and shift the arrival time estimate accordingly. Even though the fish tag receiver is 5 times less Doppler sensitive than the RAFOS detector, one knot of relative motion still causes a time-of-arrival error of 0.9 seconds, which translates into a distance error of 0.75 nautical miles. Furthermore, if the relative source versus receiver velocity varies noticeably over the 32 second signature duration, the sound signature will be distorted, which in turn reduces the number of matched pairs registered by the correlation counter. Both of these effects scale as the inverse signal bandwidth. Another reason for diminished correlation peaks is the random time or phase shift between received and stored signal pattern. This alignment error is due to the discrete time nature of the output signal and scales as the receiver sampling period.

Figure 4 illustrates the relationship between correlation strength and signal swing. The plot shows minima, mean and maxima of 12 recorded correlation values per applied signal swing. To be able to precisely control the input level, we again fed the output of a signal generator directly to the preamplifier input of the analog receiver. Intersecting the line of mean correlation peaks in **Figure 4** with the detection threshold (dashed line) reveals a receiver sensitivity of approximately 180 nV. This is 2.2 times or 7 dB less than the equivalent receiver input noise voltage. The observed correlation ceiling near a value of 0.8 is due to the afore mentioned random alignment error between the actually received signature and the stored replica.

3d. The tag clock

The key to most electronic tracking systems, including GPS, is accurate timing, more specifically, accurately recording the arrival times of characteristic patterns emitted by multiple sources at known locations. Knowing the signal propagation speed and the travel times of all detected signals, one can infer the position of the receiver via triangulation (Eriksson, 1994). To obtain the most accurate estimate for position, source and receiver clocks have to be perfectly synchronized. Keeping source and receiver synchronized over long time spans without periodic corrections, however, remains a serious issue: a static clock error of only 1 part-per-million (ppm) accumulates to a deviation of 32 seconds over one year.

Since the fish tag is severely limited in energy capacity, it employs a commercial 32.768 kHz watch crystal oscillator with a current drain of just 300 - 500 nA. This crystal oscillator is manufactured for room temperature operation and thus features a zero temperature gradient near 25°C rather than 10-12°C, which would be more desirable for underwater applications. In addition, its nominal frequency can deviate by as much as ±20 ppm due to variations in the production process. To counter this, the fish tag timer employs a digital correction unit, which allows adjusting for offset errors and compensating for the expected temperature deviations. The 6-bit digital correction scheme consists of two parts, a static correction to eliminate the offset caused by fabrication process variations and a dynamic portion to compensate for the temperature induced frequency deviations. Compensating for a possible worst-case error of ±45 ppm (static plus dynamic) requires a minimum correction step of 1.4 ppm. We have selected 1.9 ppm, since this corresponds to adding or subtracting one clock cycle in 2^{19}, which, for the 32.768 kHz clock, equates to one correction per 16 seconds so that the residual errors are equally distributed between ±0.95 ppm. **Figure 5** graphically illustrates the applied digital correction scheme.

In a dynamic environment, the cumulative timing error should approach zero, since each temperature causes a different error uniformly distributed between the two bounds of ±0.95 ppm. Realistically, each oscillator will deviate slightly from its expected temperature characteristic, leaving a residual cumulative error. Furthermore, in a scenario where the temperature remains constant over long periods of time, cumulative errors can become quite prominent. This scenario could arise in deep water fish studies, where temperature is rather stable. But there are two ways clock errors can be reduced retroactively. First, when a tag is recovered, the measured clock error coupled with a post-calibration of the crystal's temperature dependence can lead to an improved clock error history. The second approach, which is often used in RAFOS, uses travel time differences from three sound sources to determine position hyperbolically. Knowing position, one can then retroactively determine the clock correction needed to obtain the right travel times (Blanchard, 1991).

To validate the expected behavior of the cumulative timing error, we recorded temperature and acoustic arrival times with two of our prototype tags over a period of 10 days. Temperature was recorded hourly, but the acoustic stimulus was applied only once a day. To obtain different temperature profiles, we kept one tag at room temperature while the other one was intermittently exposed to a colder environment.

The top plot in **Figure 6** displays the two recorded temperature profiles while the bottom one reveals the corresponding cumulative timing errors. In spite of the two distinctly different temperature records, the arrival time errors recorded during this 10-day test stayed within bounds of ±1 ppm. Without the digital clock correction, the cumulative timing error of either tag would likely have amounted to several seconds over the 10-day test period.

Figure 7 presents a micrograph of the core microchip. This 1.5x1.5 mm die, referred to as fish chip, accommodates all basic functional units of the tag, including the sound arrival time detector, the temperature sensor, the pressure sensor interface, the 10-bit dual-slope analog-to-digital converter, the clock tuning circuitry and the central controller responsible for the timely execution all sampling tasks and data transfers to and from the tag. To minimize the crosstalk between analog and digital building blocks, all analog functions have been realized inside a relatively narrow column on the right side of the depicted die, surrounded by protective guard rings. Most of the remaining chip area is filled by two identical digital correlator circuits and a common random access memory (RAM), which archives the selected sound signature (Pattern RAM) and temporarily stores the incoming bit stream generated by the receiver (Hydro RAM). By simultaneously reading the Pattern RAM in forward and backward mode and feeding each data stream to a designated correlator, the chip executes two concurrent signal arrival time detections. This 2-way discrimination does not require physically different sound sources; they simply have to be instructed to emit the selected signal pattern in forward or time reversed mode, respectively. A potential benefit of employing both ascending and descending frequency modulation is that the Doppler shift will be in opposite directions. The average time of arrival will remove the Doppler effect while the difference between the two will provide a measure of fish tag speed in direction of the sound source.

3e. Tag Assembly

From a conceptual perspective, the tag assembly is a rather straightforward matter. Unfortunately, this statement does not equally apply to the actual physical assembly. The fish chip, housed in a quadrature leadless carrier of just 3 mm side length, is surface mounted on a tiny printed circuit board (PCB) together will the other electronic components, i.e., the watch crystal oscillator, the nonvolatile memory chips and 3 filter capacitors. This PCB is only 8 mm wide and fits tightly inside the hydrophone cylinder. The circular pressure sensor board is attached perpendicular to the PCB and forms one of the two side plates of the cylindrical tag. The other components of the device are a pair of button cell batteries with connecting wires and the copolymer hydrophone. All components and the final tag are depicted in **Figure 8.** The top layer of the tiny PCB on the top left accommodates the custom fish chip and one nonvolatile memory chip. The hidden bottom layer houses a second memory chip, the watch crystal oscillator and the 3 filter capacitors. The fully assembled tag, depicted on the right, is 4.8 cm long, has a volume of 5.8 cm^3 and weighs 8.4 g. Its net weight in seawater is 2.5 g. The component cost for the depicted tag, when purchased for a volume in the low hundreds, is around $ 150. If one adds another $ 50 to include the tag assembly, the production cost amounts to approximately $ 200 per unit. This is to roughly 4% of the cost of a RAFOS float.

3f. Sampling Protocol and Power

The tag's sampling protocol is defined by 4 parameters. Temperature, pressure and battery voltage sampling is determined by tow values, the activation time **Ta** (the time elapsed between programming and start of the sampling mission) and the time **Ts** between 2 sensor sampling instances. The remaining 2 parameters define frequency and length of the acoustic window. Since the acoustic position is likely to be assessed less frequently than temperature, pressure and battery voltage, the time between two acoustic tracking events has been defined as a power of 2 multiple, i.e., $\mathbf{2^M}$, of the sensor sampling interval **Ts**. The user selects the exponent **M** as a whole number between 0 and 7. The parameter **Tw**, finally, indicates the length of the acoustic listening window. **Table 1** lists range and step size of each of the three crucial timing parameters **Ta**, **Ts** and **Tw**. It also summarizes the capabilities of the 3 sensors for temperature, pressure and battery voltage by listing range and resolution of each.

Prior to each mission, the user uploads the 4 sampling protocol parameters **Ta**, **Ts, Tw** and **M** from a graphical user interface (GUI) on a laptop or tablet. The GUI also asks for two digital corrections compensating for the thermal sensor offset and the static frequency deviation of the crystal oscillator, respectively. These values have been obtained from the preceding pre-calibration procedure. Upon completion of the programming phase, the wire bound interface to the host is removed so that the tag can be sealed and made ready for deployment.

Frequency and duration of the acoustic tracking have a major impact on the power budget. The supply current recorded during active tracking, i.e., the time while the tag listens for a sound signature, ranges between 20-30 μA. To illustrate the power usage, let us assume a scenario where a user programs the tag to assess geographic position once per hour with an acoustic listening window of 6 minutes. The additional average current drain then amounts to 2-3 μA (1/10 of the above). Selecting the more conservative number and combining it with the observed standby current of 1.5 μA yields a total current drain of approximately 4.5 μA. Combining this average power drain with the 80 mAh charge stored in each of the two series connected button cell batteries results in an active tag lifetime of 17778 h or almost exactly 2 years. Assessing position and sampling temperature, pressure and battery voltage once an hour for 2 years fills 97% of the available 4 Mb memory space. Alternatively, recording position a dozen times per day while sampling temperature, pressure and battery voltage every 15 minutes fills the memory in 682 days, but consumes only 56% of the available battery energy. Since sampling, digitizing and archiving temperature, pressure and battery voltage is accomplished in less than 0.2 seconds, the computational power exerted during these events is practically irrelevant.

4. Field Test Results

To assess the feasibility and validate the performance of the fish tag under development, a series of field tests have been conducted during the course of this project. The first one was a preliminary test designed to evaluate the critically important analog preamplifier and the potential tracking range. In this experiment, both source and receiver (the preamplifier and a commercial digital recording device) were positioned below the surface mixed layer at ~40 and 30 m, respectively, on the New England shelf south of Nantucket (Fischer, 20006). The sound source was operated at the peak power of 180 dB re 1μPa @ 1m for all transmissions. The data collected during this early field experiment showed that the preliminary receiver could repeatedly detect the RAFOS signature at the farthest site 70 km from the acoustic source. The spectral analysis of the data recorded at the most remote site revealed a surprisingly robust in-band signal-to-noise ratio of approximately 6 dB.

A second comprehensive field test took place in September 2015 at a location some 40 km south of the Eastern tip of Long Island. This site provided a relatively uniform water depth of approximately 60 m. At that time, we were not yet ready with final tags as depicted in **Figure 8**. Instead, we mounted 4 fish chips on larger PCBs housed inside 4 PVC cylinders with a volume of 2.2 liter each. The polyurethane coated copolymer hydrophones were attached to the bottom plate of each cylinder with wires connected to the fish chip. This assembly provided full thermal and acoustic functionality.

The logistics of the experiment were rather simple. The 4 PVC cylinders, or pods, were attached to a rope hanging below a free-floating surface drifter. The 4 pods were placed at depths of 10 m, 20 m, 30 m, and 40 m, respectively. The host vessel, the Endeavor, then steamed ~4 km northeast of the free drifting hydrophones for a first transmission test. The sound source was lowered from the stern of the Endeavor to a depth of approximately 15 m and activated manually 6 times, once per minute, each time emitting a linear frequency sweep (“pong”) at maximum power from 260.5 Hz to 263.5 Hz over 32 seconds. This procedure was repeated at a second test site at a distance of 17 km in the same direction. We transmitted 7 pongs at this second site. Unfortunately, one pod reset before deployment, and another leaked, but the pods, at 10 m and 40 m depth, performed as intended. Their acoustic recordings are summarized in **Table 2**. All transmitted signals were detected with distinct correlation peaks at both recording sites. The scatter in arrival times recorded at either location can be attributed to the manual activation of the sound source since it could not be programmed to transmit on such a fast schedule. Similarly, the approximately 0. 2 second longer travel times recorded by Pod 2 are most likely due to the manual initialization of the clocks, i.e., receiver 2 was initialized 0.2 seconds earlier than its counterpart. The strong correlation values recorded at either site are very encouraging and hint at a significantly larger signal propagation range than 17 km.

To further validate the proper operation of the final tag design, we conducted one more field test with a few completely assembled tags south of the Mississippi delta in the Gulf of Mexico. The test was carried out following the same protocol applied during the previous field experiment. The tags were attached to the ends of two approximately 30 m long ropes, which were tied to two

surface drifting buoys equipped with a GPS tracker. The sound source was then lowered repeatedly to a depth of approximately 25 m from the Starboard side of the Endeavor at various distances starting at ~130 km. Two of the pods employed in the previous field test served as end-of-rope weights and reference data collectors. **Figure 9** shows all signal paths between drifter and respective pong site.

The tags and pods recorded an almost uniform water temperature near 27°C during the 40-hour test period. This provided for less than ideal acoustic conditions, since a warm surface layer tends to refract sound away from the surface. But a thin fresh water lens of Mississippi origin created a shallow surface sound channel such that transmissions could be detected as far as 60 km away. It is therefore not surprising that none of the tags and pods detected a signal emitted from any of the three farthest source sites (sites S1-S3 in **Figure9**) located 72 -130 km away. The source pressure level, measured with a calibrated hydrophone, was 180 dB re 1 μPa @ 1 m.

Figure 10 shows the averages of all recorded signal propagation times as a function of sound source distance as deduced from GPS data. The insert at the bottom right lists GPS distance, number of detected signals, average signal propagation time and standard deviation for all sites that yielded successful recordings.

Several interesting points can be made. First, the spread in signal propagation times is remarkably small, 0.053-0.132 seconds. Excluding variations in the physical propagation path, this would translate to a distance resolution of better than 200 m, which is not far from the theoretical best of 47 m resulting from the 32 Hz sampling clock of the arrival time detector. Second, the apparent variations in sound speed partially stem from uncertainties in distance due to the 5-minute resolution of the drifter GPS data (we did not interpolate). Third, it is strange that the best speed of sound to reconcile computed distance with measured travel time is not what might be expected on the basis of our estimates of surface/near surface temperature and salinity (=1523 m/s for 25 PSU, 25°C, 20 m) along the signal propagation path (Dushaw et al., 1993). Instead, the best fit for the data displayed in **Figure 10** is around 1490 m/s (~2% less) with some uncertainty due to the paucity of data at the greater ranges. All travel times are relative to measured arrival times when the tags and pods were at zero m distance (placed inside the sound source on deck) immediately after retrieval.

5. Summary

We have described the development and validation of a new archival fish tag designed to track marine animals, whether in the water column (nekton) or on the bottom (benthic fish and crustaceans). The tag, similar in size to other archival tags, operates according to standard RAFOS tracking principles: it detects and records the arrival times of signals transmitted from moored sound sources. Navigational accuracy is determined by how well source and receiver clocks are aligned. Timing errors in the tag are kept quite small by compensating for the temperature dependent drift of the crystal clock during mission. Listening schedules can be set up according to tracking needs. Pressure and temperature can be sampled more frequently (up to 128 times) than searching for sound signatures to better resolve vertical movements and diurnal

behavior of the tagged species. Power to the fish tag comes from two button cell silver-oxide batteries, which enable an active tag lifetime of approximately two years.

Previous field studies involving archival tags have shown that tag return rates between 5-10% are possible depending on species and location. While this is encouraging, the need to retrieve the tag remains a major obstacle. If the presented technology is ported to larger, intermittently surfacing sampling platforms, however, it becomes possible to add a satellite transmitter, which can upload the archived data at opportunistic times. This feature as well as wireless device programming are primary targets in future developments of this technology. As a first step in this direction, the fish chip technology is being ported to the next generation RAFOS float, and it can readily be employed on gliders and AUVs for interactive navigation. Since the fish chip requires virtually no power, it can also be added to long-range missions such as Argo floats, provided there is interest in tracking these with greater spatial resolution.

Acknowledgements

This work has been supported by subsequent NSF/OTIC awards 0326907, 1061083 and 1435698. The authors would like to thank the following people who contributed in no minor way to the success of this endeavor: Tanya Wang for her skillful assembly of the final tags, Michael Platek for the assembly of the test pods, Bill Fanning for his technical support at sea and the captain and the crew of the RV Endeavor from which all field work was done. Funding by the Rhode Island Endeavor Program for two cruises is gratefully acknowledged.

References

Blanchard, W. F. (1991). Air Navigation Systems Chapter 4. Hyperbolic Airborne Radio Navigation Aids - A Navigator's View of their History and Development, The Journal of Navigation, 44, (3), 285-315.

Block, B.A., H. Dewar, S.B. Blackwell, T.D. Williams, E.D. Prince, C.J. Farwell, A. Boustani, S.L.H. Teo, A. Seitz, A. Walli and A. Fudge, 2001. Migratory movements, depth preferences, and thermal biology of Atlantic bluefin tuna. Science 293(5533), 1310-1314.

Bower A. S., L. Armi, I. Ambar, 1995: Direct evidence of eddy formation off the southwestern coast of Portugal. *Deep-Sea Res. I* 42, 1621-1630.

Crols, J., M. Steyaert, 1994: Switched-Opamp: An Approach to realize full CMOS Switched-Capacitor Circuits at very low Power Supply Voltages. *IEEE J. of Solid-State Circuits*, 29, 936-942.

Dushaw, B. D., P.R. Worcester, B.D. Cornuelle, B.M. Howe, 1993: On Equations for the Speed of Sound in Seawater. *J. Acoustic Soc. Amer*., 93, 255-275.

Eriksson, H., P.O. Börjesson, P. Oding and N-G. Holmer, 1994: A robust Correlation Receiver for Distance Estimation. *IEEE Transactions on Ultrasonics, Ferroelectrics and Frequency Control*, 41, 596-603.

Fischer, G., S. Lee, M. Obara, P. Kasturi, H.T. Rossby and C.W Recksiek, 2006: Tracking Fishes with a microwatt acoustic Receiver – An archival Tag Development. *IEEE J. Oceanic Engineering*, 31, 975-986.

Fischer G. and F. Luo, 2012: Jitter in ultra-low Power Audio-Range PLLs. *Proc. IEEE MWSCAS'12*, Boise, Idaho, 550-553.

Gazit, T., Apostle, R., Branton, R., 2013, Deployment, tracking and data management technology and science for a global ocean tracking network, J. of Intl. Wildlife Law and Policy 16: 112-127.

Gunn, J. and J. Hartog, 1999. Archival tag project report. Southern Bluefin Tuna Recruitment Monitoring and Tagging Program: Workshop Rep. 11, CRIMP, 5 pp.

Harrison, C. H., 1996: Formulas for ambient Noise Level and Coherence. *J. Acoustic Soc. Amer.*, 2055–2066.

Metcalfe, J.D., G. P. Arnold and B. H. Holford, 1994. The migratory behavior of plaice in the North Sea as revealed by data storage tags. ICES Council meeting 1994/Mini11, International Council for the Exploration of the Sea, 13 pp.

Parvin, S. J., Nedwell, J.R., Harland E, 2007, Lethal and physical injury of marine mammals, and requirements for Passive Acoustic Monitoring, *Subacoustech Report No. 565R0212*, 36 pp.

Rossby, H.T., A. Voorhis and D. Webb, 1975. A quasi-Lagrangian study of mid-ocean variability using long-range SOFAR floats. *J. Mar. Res*., 33(3), 355-382.

Rossby, H. T., D. Dorson and J. Fontaine, 1986: The RAFOS System. *J. of Atmos. Oc. Tech.* 3, 672-679.

Rossby, H. T., J. Ellis and D.C. Webb, 1993: An efficient Sound Source for wide-area RAFOS Navigation. *J. Atmos. Oc. Tech.*, 10, 397-403.

Rossby, H. T., 1996. The North Atlantic Current and Surrounding Waters: At the Crossroads, *Reviews of Geophysics*, 34,4, 463-481.

Rossby, H. T., 2007. Evolution of Lagrangian methods in Oceanography. Ch. 1 in Lagrangian Analysis and Prediction in Coastal and Ocean Processes. Cambridge University Press.

Schneider, M. C., C. Galup-Montoro, 2010: Fundamentals of sampled-data Circuits. *Cambridge University Press*, 404-451.

Urick, R. J., 1983: Principles of underwater sound. Peninsula Publishing, Los Altos, CA 423 pp.

Urick, R. J., 1984: Ambient Noise in the Sea. Undersea Warfare Technology Office, Naval Systems Command, Department of the Navy, Washington D.C, 194 pp.

VEMCO, 2009, VEMCO Acoustic Telemetry – New User Guide, DOC-004934-01, www.vemco.com, 1-22.

Vittoz E. A., O. Neyroud, 1979: A low-voltage CMOS Bandgap Reference," *IEEE J. of Solid-State Circuits*, 14, 573-577.

Wenz, G. M., 1962: Acoustic ambient Noise in the Ocean. *J. Acoustic Soc. Amer.*, 34, 1946-1956.

Tables

Table 1. Pertinent fish tag parameters.

Sampling Protocol			Sensors		
Param.	**Range**	**Step**	**Type**	**Range**	**Resolution**
Ta	24 d	1 s	Temp.	45°C	0.044 ± 0.004°C
Ts	18 h	1 s	Pressure	300 PSI	0.75 ± 0.25 PSI
Tw	34 m	1 s	Battery	3.6 V	3.45 ± 0.15 mV

Table 2. Acoustic data recorded during field test off Long Island.

Site	Pong	Pod 1 (10 m depth)		Pod 2 (40 m depth)	
		T_p [s]	Corr.	T_p [s]	Corr.
1 **4.8 km**	1	2.47	.336	2.72	.395
	2	3.41	.289	3.66	.340
	3	3.03	.293	3.03	.375
	4	3.38	.363	3.56	.402
	5	3.34	.324	3.66	.336
	6	3.22	.355	3.28	.430
Mean		**3.142**	**0.327**	**3.318**	**0.380**
St. Dev.		**0.357**	**0.031**	**0.383**	**0.037**
2 **17.0 km**	1	10.94	.293	11.03	.199
	2	11.00	.363	11.38	.344
	3	11.56	.301	11.66	.313
	4	11.31	.309	11.56	.336
	5	10.56	.352	10.84	.329
	6	11.50	.305	11.81	.406
	7	11.00	.402	11.22	.426
Mean		**11.12**	**0.332**	**11.36**	**0.336**
St. Dev.		**0.353**	**0.041**	**0.349**	**0.073**

Figure Captions

Figure 1. Basic functional blocks of the fish tag. All components inside the dark gray area are housed on the application specific integrated circuit (ASIC).

Figure 2. Spectral response of receiver filter cascade in presence of a 262 Hz sinusoidal input of 500 nV amplitude. The spectrum has been computed via a 1-million-point FFT using a sampling rate of 10 kHz. This yields a spectral resolution of 0.01 Hz.

Figure 3. The top left plot displays the response of the receiver to an ideal rms input voltage of 180 nV. The bottom left plot reflects a scenario with two 32-second-long input signals spaced 0.4 seconds apart in time. Both inputs feature rms voltage of 180 nV and an equivalent noise component of 360 nV, representing an SNR of -6 dB. The plots on the right show the corresponding correlator function (top) and the 2 signal arrival time estimates deduced by the peak detector (bottom).

Figure 4. Recorded correlation strength versus receiver input voltage. The plot marks minimum, maximum and mean of 12 consecutive recordings conducted per input signal level.

Figure 5. Illustration of applied digital correction scheme to mitigate the temperature induced frequency deviations of the watch crystal.

Figure 6. Temperature recordings during 10-day timing test (top) and corresponding cumulative clock error (bottom) assessed one a day.

Figure 7. Micrograph of fish chip. The annotations reveal the pertinent functional building blocks (die size: 1.5 mm x 1.5 mm).

Figure 8. Fish tag components vis-a-vis a US dime (center top) and an assembled tag on the right.

Figure 9. Test site some 50 km SW of Mississippi delta. The tracks of the two surface drifters are marked by bold lines. The thin lines reveal the acoustic signal paths from the various sound source locations (S1-S9) to the two drifter positions at the time of the sound transmissions. The contours indicate water depth in steps of 100 m (dark to light).

Figure 10. Average signal propagation times versus distance as recorded by the tags and pods during the field test SW of the Mississippi delta. The insert lists distance, number of detections per location, average propagation time and corresponding standard deviation.

Figures

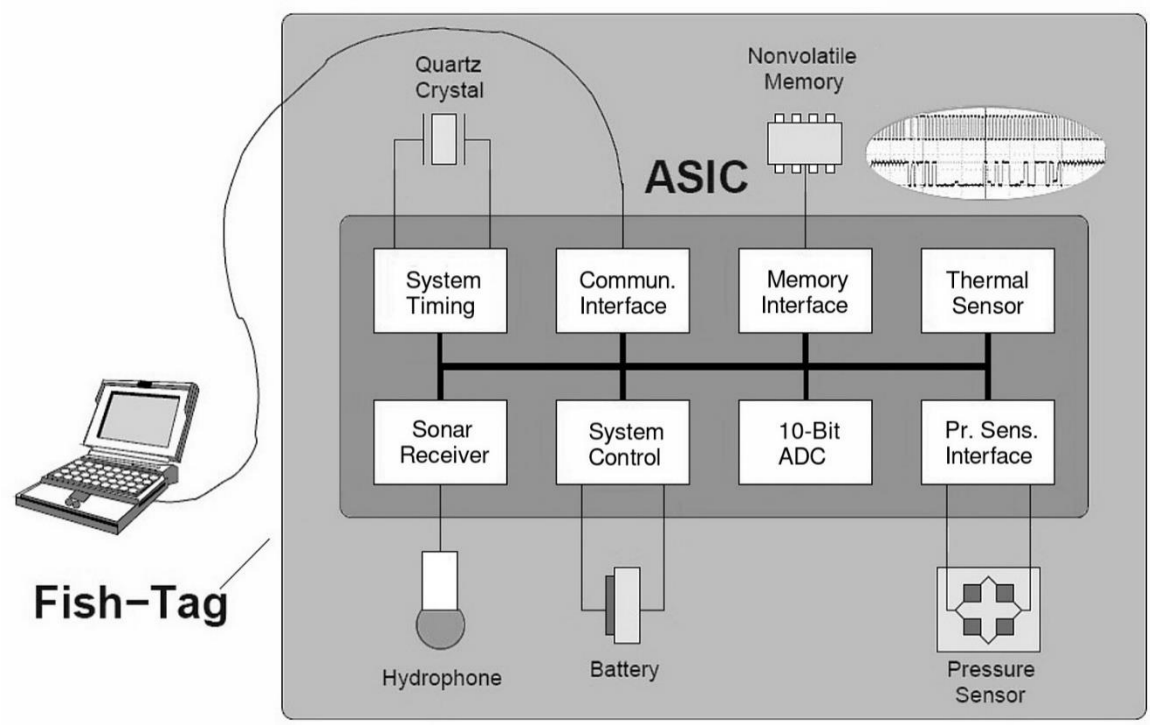

Figure 1. Basic functional blocks of the fish tag. All components inside the dark gray area are housed on the application specific integrated circuit (ASIC).

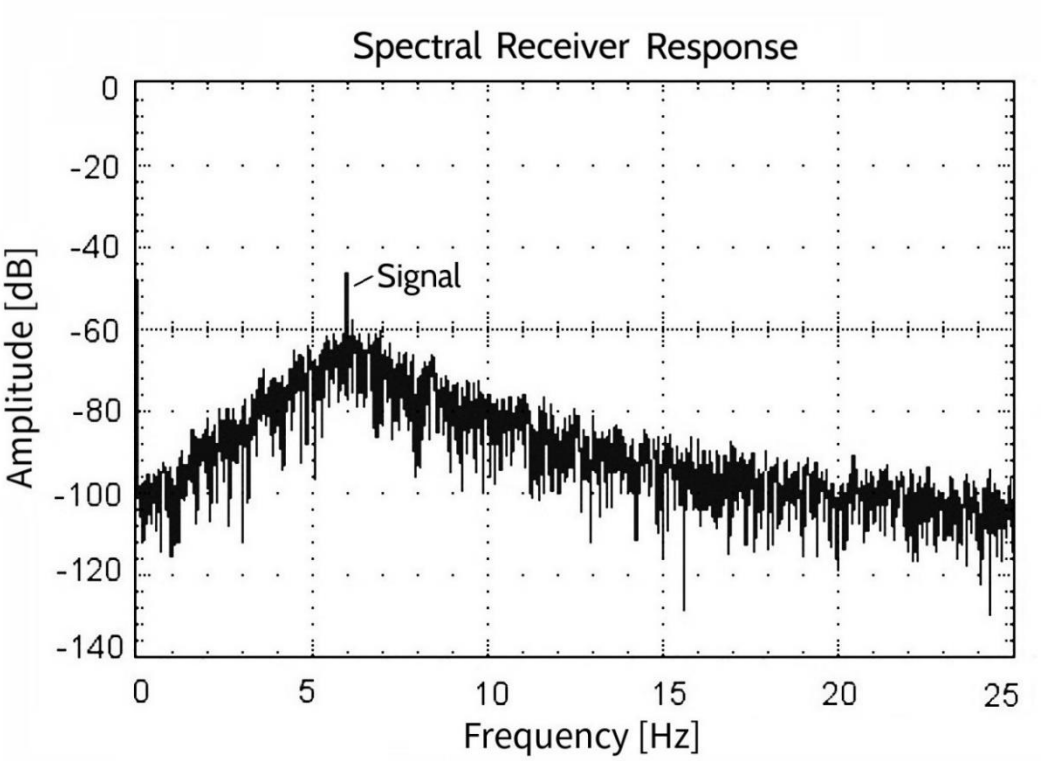

Figure 2. Spectral response of receiver filter cascade in presence of a 262 Hz sinusoidal input of 500 nV amplitude. The spectrum has been computed via a 1-million-point FFT using a sampling rate of 10 kHz. This yields a spectral resolution of 0.01 Hz.

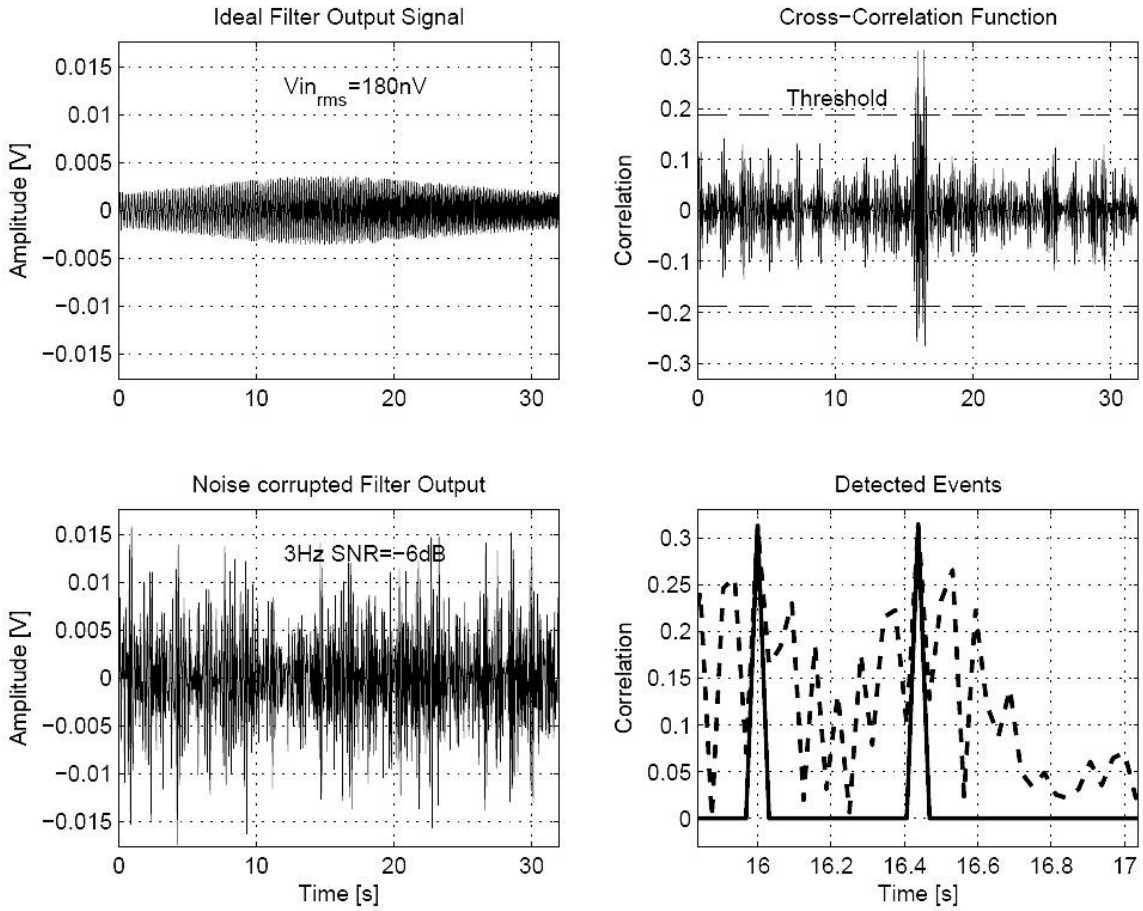

Figure 3. The top left plot displays the response of the receiver to an ideal rms input voltage of 180 nV. The bottom left plot reflects a scenario with two 32-second-long input signals spaced 0.4 seconds apart in time. Both inputs feature an rms voltage of 180 nV and an equivalent noise component of 360 nV, representing an SNR of -6 dB. The plots on the right show the corresponding correlator function (top) and the 2 signal arrival time estimates deduced by the peak detector (bottom).

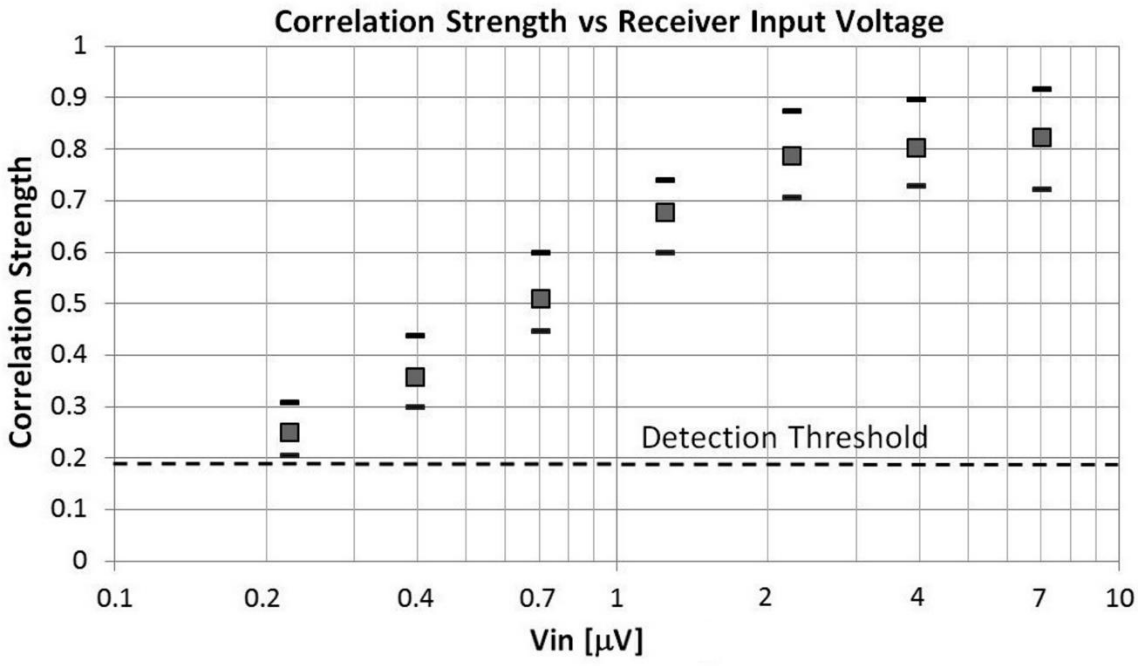

Figure 4. Recorded correlation strength versus receiver input voltage. The plot marks minimum, maximum and mean of 12 consecutive recordings conducted per input signal level.

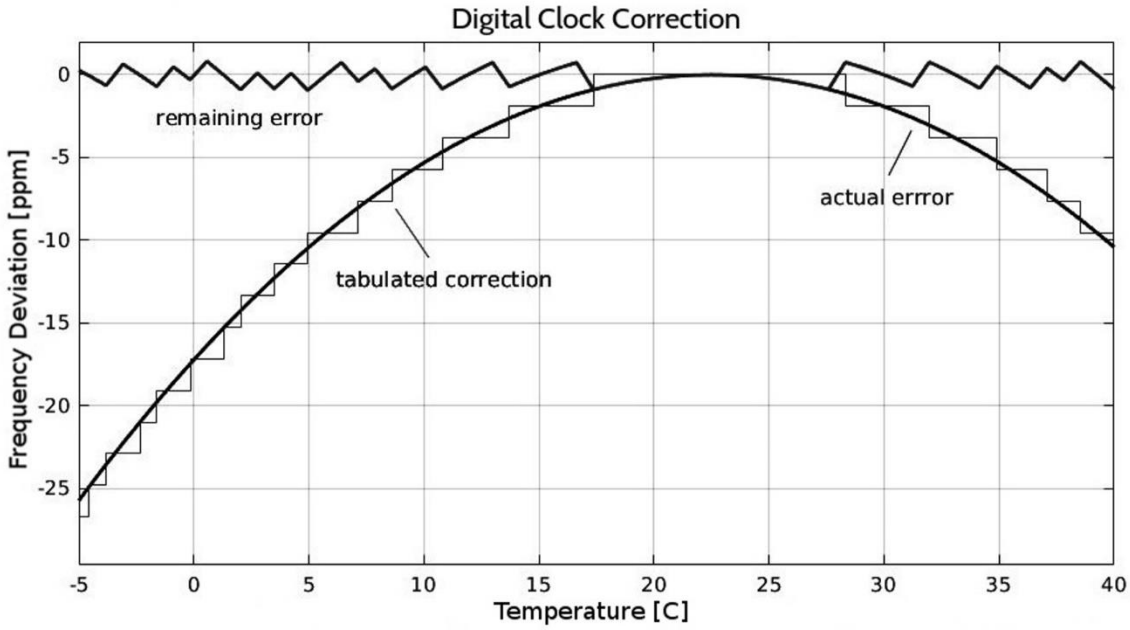

Figure 5. Illustration of applied digital correction scheme to mitigate the temperature induced frequency deviations of the watch crystal.

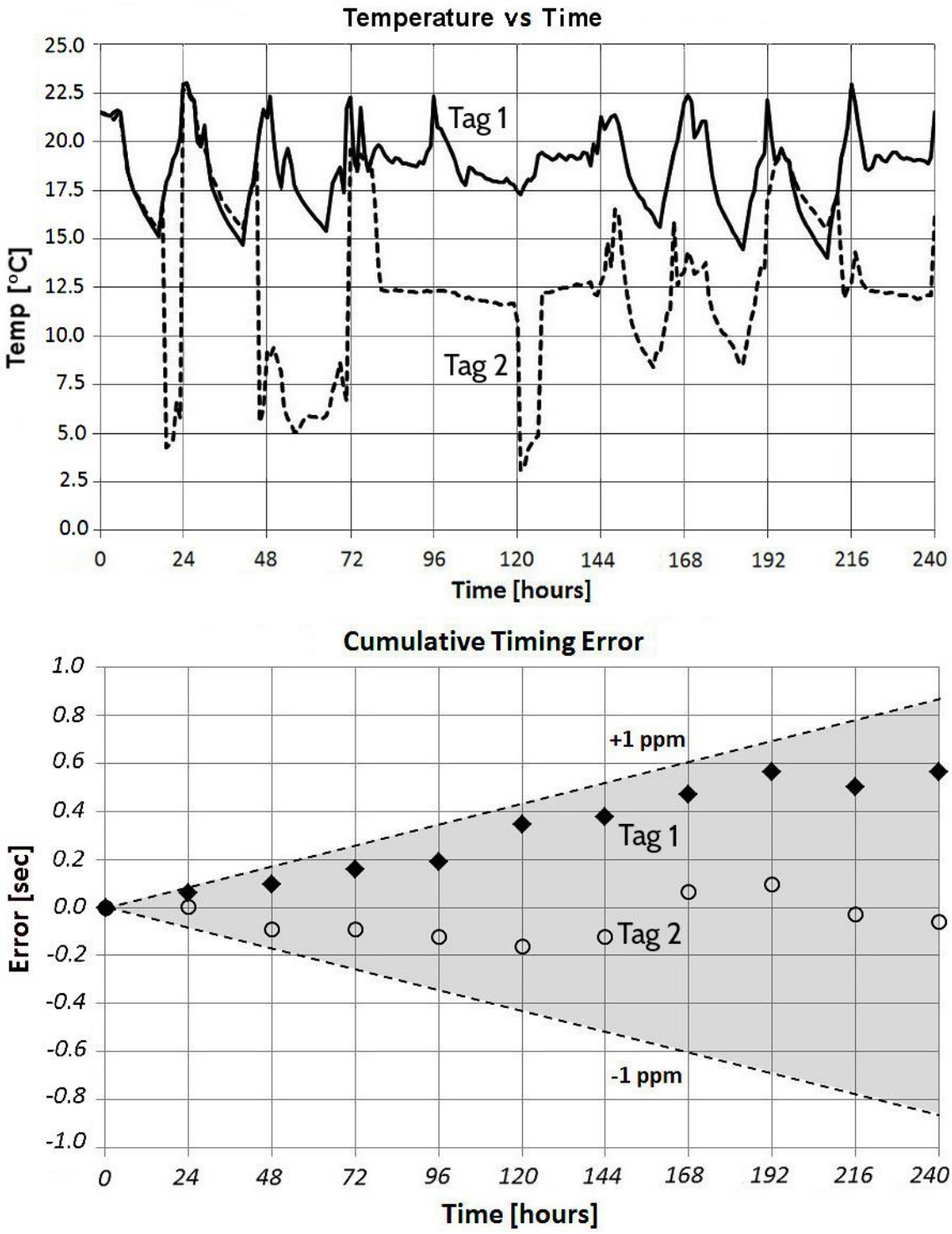

Figure 6. Temperature recordings during 10-day timing test (top) and corresponding cumulative clock error (bottom) assessed one a day.

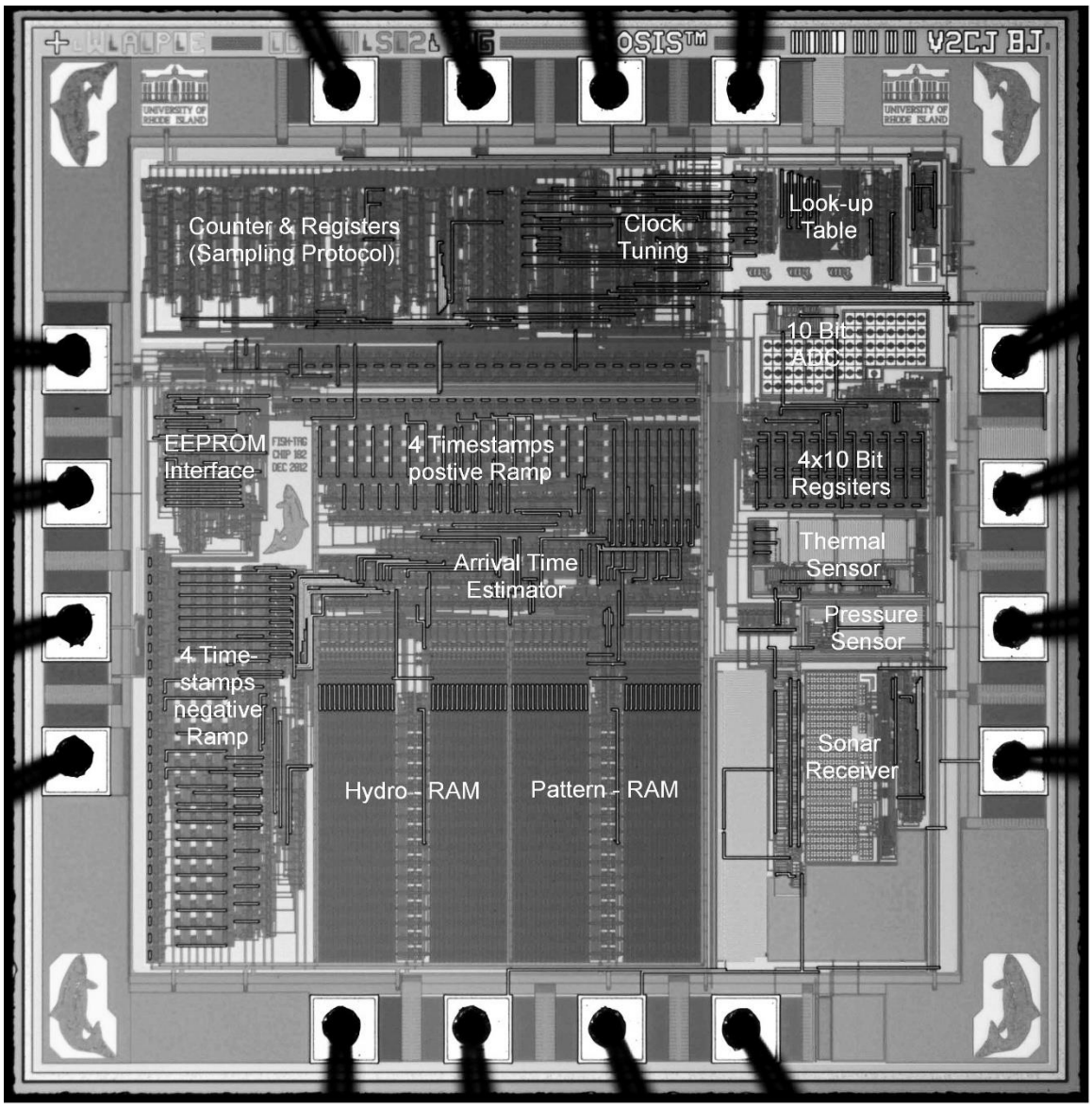

Figure 7. Micrograph of fish chip. The annotations reveal the pertinent functional building blocks (die size: 1.5 mm x 1.5 mm).

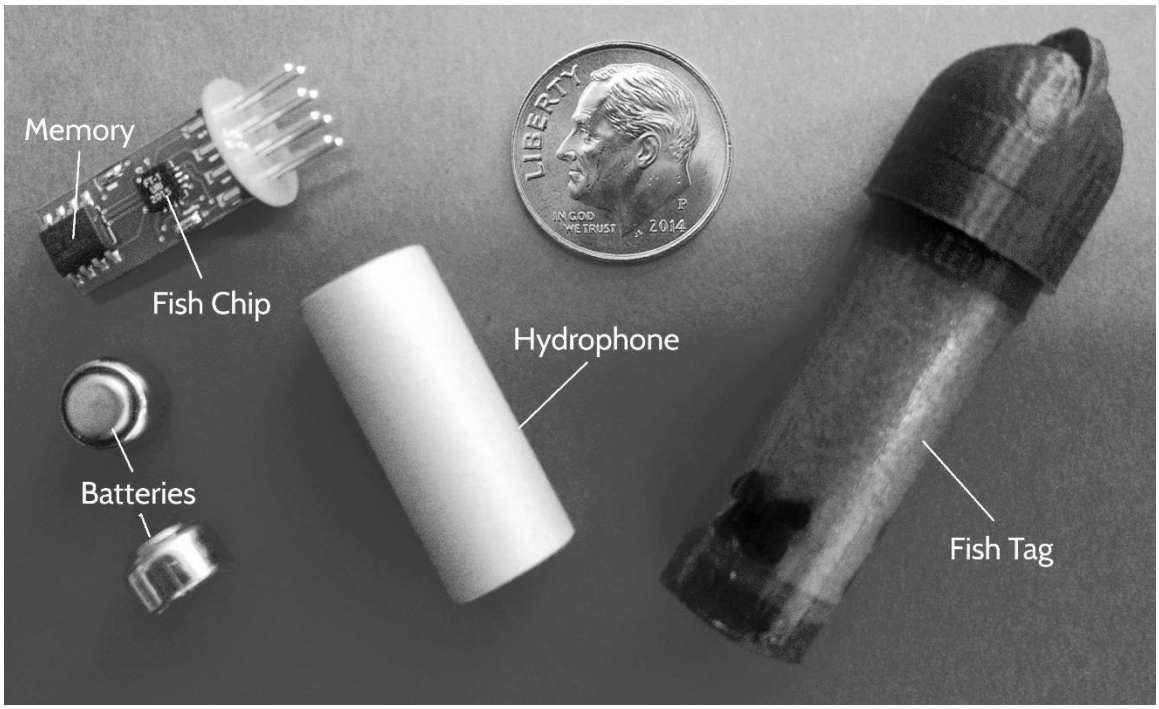

Figure 8. Fish tag components vis-a-vis a US dime (center top) and an assembled tag on the right.

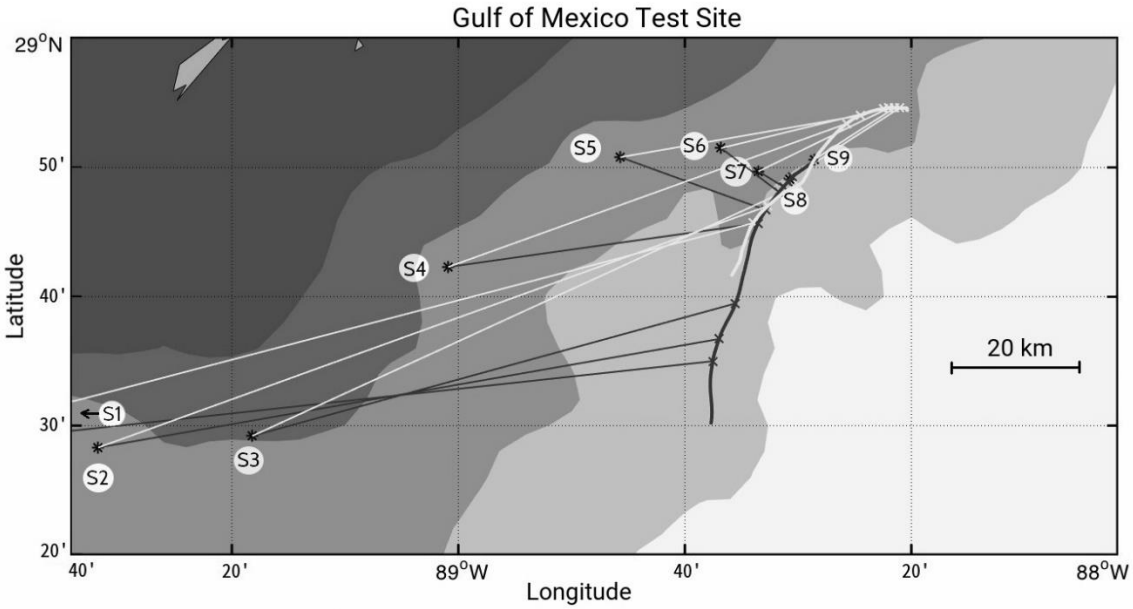

Figure 9. Test site some 50 km SW of Mississippi delta. The tracks of the two surface drifters are marked by bold lines. The thin lines reveal the acoustic signal paths from the various sound source locations (S1-S9) to the two drifter positions at the time of the sound transmissions. The contours indicate water depth in steps of 100 m (dark to light).

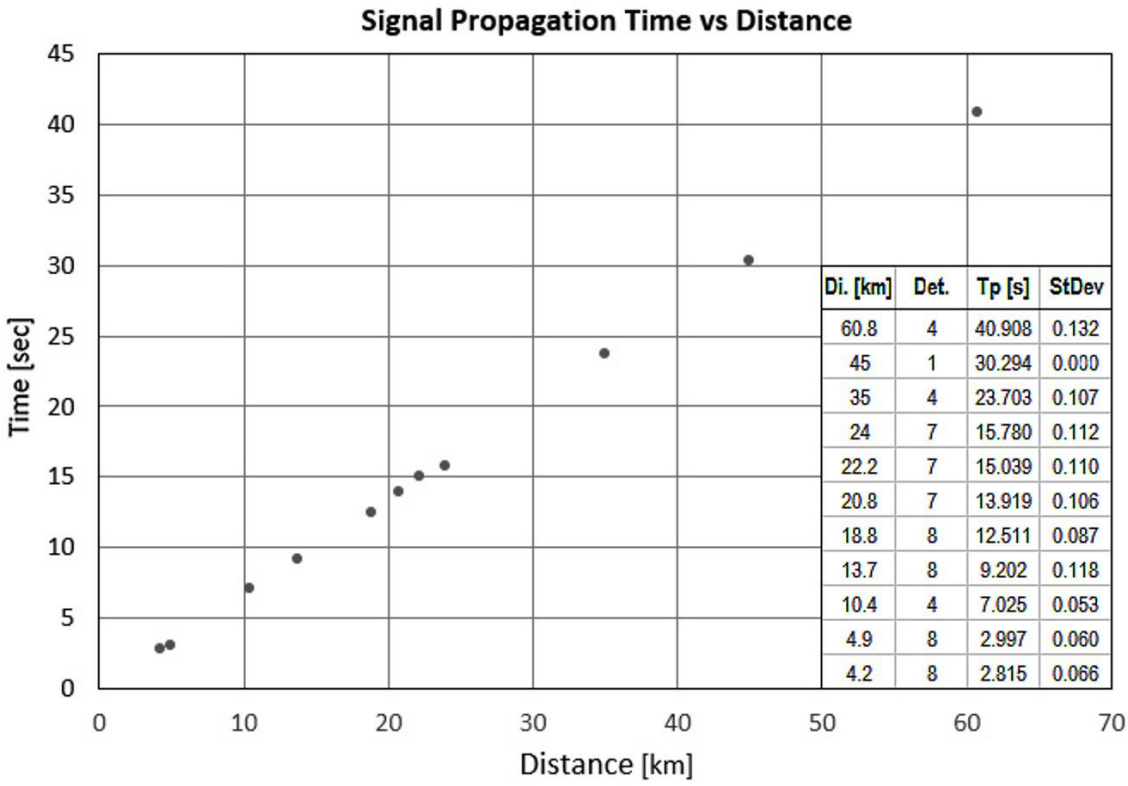

Di. [km]	Det.	Tp [s]	StDev
60.8	4	40.908	0.132
45	1	30.294	0.000
35	4	23.703	0.107
24	7	15.780	0.112
22.2	7	15.039	0.110
20.8	7	13.919	0.106
18.8	8	12.511	0.087
13.7	8	9.202	0.118
10.4	4	7.025	0.053
4.9	8	2.997	0.060
4.2	8	2.815	0.066

Figure 10. Average signal propagation times versus distance as recorded by the tags and pods during the field test SW of the Mississippi delta. The insert lists distance, number of detections per location, average propagation time and corresponding standard deviation.

1